



## Precise heavy-quark masses

S. Moch

*II. Institut für Theoretische Physik, Universität Hamburg  
Luruper Chaussee 149, D-22761 Hamburg, Germany*

---

### Abstract

We report on determinations of the running masses for charm- and bottom-quarks from deep-inelastic scattering reactions and for the top-quark from hadro-production of top-quark pairs. The running masses in the  $\overline{\text{MS}}$  scheme can be extracted with good precision at next-to-next-to-leading order in QCD. In the global fits to data the full correlations of the extracted mass parameters with the parton distributions in the proton and with the strong coupling constant  $\alpha_s$  are kept. For charm- and bottom-quarks the method provides complementary information on these fundamental parameters from hadronic processes with space-like kinematics. The measured top-quark mass is confronted with the Monte Carlo top-quark mass parameter determined from a comparison to events with top-quark decay products. The Monte Carlo mass is not identical with the pole mass. Its translation to the pole mass scheme introduces an additional uncertainty of the order of 1 GeV.

*Keywords:* heavy-quark hadro-production, heavy-quark structure function in deep-inelastic scattering, charm-quark mass, bottom-quark mass, top-quark mass, running masses in  $\overline{\text{MS}}$  scheme

---

### 1. Introduction

Quark masses are fundamental parameters of the gauge theory of the strong interactions, Quantum Chromodynamics (QCD). They are, however, not directly observable due to confinement. Quark masses appear in the theory predictions for cross sections or other measurable quantities and, as such, they are subject to the definition of a renormalization scheme once quantum corrections at higher orders are included. In many QCD applications the pole mass is the conventional scheme choice. The heavy-quark's pole mass  $m_q^{\text{pole}}$  is introduced in a gauge invariant and well-defined way at each finite order of perturbation theory as the location of the single pole in the two-point correlation function. The pole mass scheme is, in fact, inspired by the definition of the electron mass in Quantum Electrodynamics. For heavy quarks, however, this has its short-comings [1, 2], because due to confinement quarks do not appear as free particles in asymptotic states in the  $S$ -matrix. Therefore, the pole mass  $m_q^{\text{pole}}$  must acquire non-perturbative

corrections, because in the full theory the quark two-point function does not display any pole. This leads to an intrinsic uncertainty in the definition of  $m_q^{\text{pole}}$  of the order of  $\Lambda_{\text{QCD}}$  related to the renormalon ambiguity [3].

Fortunately, one can consider alternative definitions based on the (modified) minimal subtraction in the  $\overline{\text{MS}}$  scheme, which realizes the concept of a running mass  $m_q(\mu)$  at a scale  $\mu$  of the hard scattering in complete analogy to the treatment of the running strong coupling  $\alpha_s(\mu)$ . As a benefit, predictions for hard scattering cross sections in terms of the  $\overline{\text{MS}}$  mass display better convergence properties and greater perturbative stability at higher orders.

More generally, one can define so-called short-distance masses  $m_q(R, \mu)$ , where  $R$  is a scale associated with the scheme. The  $\overline{\text{MS}}$  mass is then just one example of a short-distance mass  $m_q(R, \mu)$  with  $R$  taken at the scale  $R \sim m_q$ . Other schemes define a so-called  $1S$  mass [4, 5] through the perturbative contribution to the mass of a hypothetical  $^3S_1$  toponium bound state

or a “potential-subtracted” (PS) mass [6]. As alternative renormalization schemes, all short-distance masses  $m_q(R, \mu)$  can be related to the pole mass  $m_q^{\text{pole}}$  through a perturbative series,

$$m_q^{\text{pole}} = m_q^{\text{MSR}}(R, \mu) + \delta m_q(R, \mu), \quad (1)$$

$$\delta m_q(R, \mu) = R \sum_{n=1}^{\infty} \sum_{k=0}^n a_{nk} \alpha_s^n(\mu) \ln^k \left( \frac{\mu^2}{R^2} \right), \quad (2)$$

with coefficients  $a_{nk}$  known to three loops in QCD [7, 8].

As quark masses are not physical observables the determination of  $m_q$  relies on the comparison of a theory prediction  $\sigma_{\text{th}}(m_q)$  for a cross section with the experimentally measured value  $\sigma_{\text{exp}}$  for a given observable and kinematics as the best fit solution to the equation  $\sigma_{\text{exp}} = \sigma_{\text{th}}(m_q)$ . The accuracy of this approach is intrinsically limited by the sensitivity  $\mathcal{S}$  of  $\sigma_{\text{th}}(m_q)$  to  $m_q$ ,

$$\left| \frac{\Delta\sigma}{\sigma} \right| = \mathcal{S} \times \left| \frac{\Delta m_q}{m_q} \right|. \quad (3)$$

Thus, for a given experimental error or a theoretical uncertainty  $\Delta\sigma$  on the cross section, the greater the sensitivity  $\mathcal{S}$  the better the accuracy for  $m_q$  can be achieved.

In this review we discuss several determinations of the running masses in the  $\overline{\text{MS}}$  scheme for charm- and bottom-quarks from deep-inelastic scattering (DIS) reactions and for the top-quark from hadro-production of top-quark pairs, which have been performed within the Collaborative Research Center/Transregio 9 (CRC/TR 9). We briefly describe the theoretical prerequisites and the global fits to data for the extraction of the running masses at next-to-next-to-leading order (NNLO) in QCD. We stress, that it is important to keep the full correlations of the extracted mass parameters with other non-perturbative parameters entering the cross sections predictions, such as the parton distribution functions (PDFs) in the proton and the reference value of the strong coupling constant  $\alpha_s(M_Z)$ .

The results reported here are quoted in the *2014 Review of Particle Physics* [9] of the particle data group (PDG) and the presentation in this article follows previous reports [10, 11] on the subject with updates.

## 2. Charm-quark mass

Cross sections for the production of heavy-quarks in DIS are particularly well suited to confront the quark mass dependence of theoretical predictions in perturbative QCD with experimental measurements in space-like kinematics. For the production of charm-quarks

in neutral (NC) or charged current (CC) DIS there exists very precise data from the HERA collider and from fixed-target experiments.

In QCD the DIS heavy-quark structure functions  $F_k$  which parametrize the hadronic cross section are subject to the standard factorization

$$F_k(x, Q^2, m_q^2) = \sum_{i=q,\bar{q},g} \left[ f_i(\mu^2) \otimes C_{k,i}(Q^2, m_q^2, \alpha_s(\mu^2)) \right](x), \quad (4)$$

where  $k = 1, 2, 3$ .  $Q^2$  and  $x$  are the usual DIS kinematical variables and  $m_q$  is the heavy-quark (pole) mass. The perturbative coefficient functions  $C_{k,i}$  are known for CC to next-to-leading order (NLO) [12, 13] and at asymptotic values of  $Q^2 \gg m_q^2$  even to NNLO [14, 15, 16]. For NC the coefficient functions have been computed approximately to NNLO [17, 18, 19, 20].

In eq. (4) we also display all dependence on the other non-perturbative parameters, i.e. the PDFs  $f_i$  for light quarks and gluons as well as the strong coupling constant  $\alpha_s$ . The conversion to the running mass definition follows the standard procedure for changing the renormalization condition, i.e.  $m_q \rightarrow m_q(\mu)$  at the respective order in perturbation theory. This has been discussed in refs. [21, 22] and the specific implementation for DIS heavy-quark production in eq. (4) has been presented in refs. [23, 24].

The parametric dependence of the DIS structure functions  $F_k$  in eq. (4) on  $m_q$  can be used for a determination of the heavy-quark mass. The sensitivity of this procedure relates directly to the corresponding uncertainty on the measurements of  $F_k$ , see eq. (3). For charm production in NC DIS the nucleon structure function  $F_2$  displays a sensitivity  $\mathcal{S} \sim 1.5$  which implies that an experimental accuracy of 4% for  $F_2$  translates into an uncertainty of 3% for the charm-quark mass [23]. With the precision of current DIS data for charm production this suggests an error on  $m_c(m_c)$  of  $O(\text{few})\%$  as the ultimate precision in the approach based on inclusive structure functions.

Starting from eq. (4) we have extracted the  $\overline{\text{MS}}$  charm-quark mass  $m_c(m_c)$  in several phenomenological studies [25, 26] (and variants [24, 27, 28]) based on world data for deep-inelastic scattering and fixed-target data as well as data from the Large Hadron Collider (LHC) for the Drell-Yan process. The use of the running mass in global analyses in the fixed-flavor number scheme (FFNS) (with  $n_f = 3$ ) is twofold. It allows for a comparison of the extracted mass parameter to the world average published by the PDG as a consistency check. In addition, due to better convergence and

greater perturbative stability of the theoretical predictions, it improves the uncertainty of heavy-quark PDFs in a global fit within the FFNS when the running mass scheme is applied.

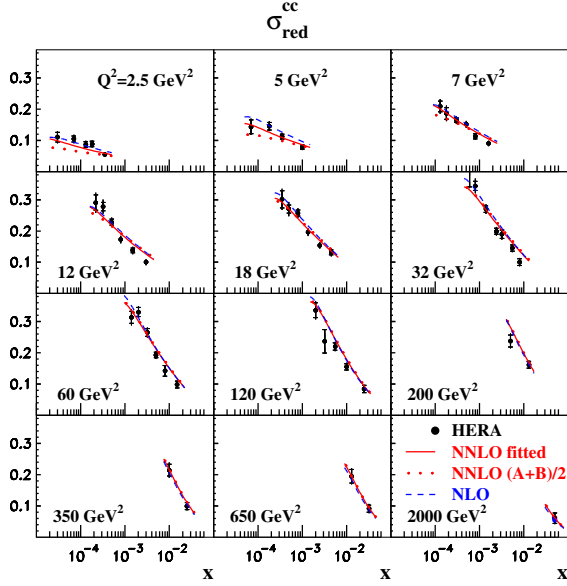


Figure 1: The combined HERA data on the reduced cross section for the open charm production [29] versus  $x$  at different values of  $Q^2$  in comparison with the result of the analysis of ref. [28] at NLO (dashed line) and NNLO (solid line). A variant of the fit based on the option (A+B)/2 of the NNLO Wilson coefficients of ref. [19], is displayed for comparison (dotted line). (Figure from ref. [28])

We have obtained [28]

$$m_c(m_c) = 1.15 \pm 0.04(\text{exp})_{-0.00}^{+0.04}(\text{scale}) \text{ GeV}, \quad (5)$$

at NLO

$$m_c(m_c) = 1.24 \pm 0.03(\text{exp})_{-0.02}^{+0.03}(\text{scale})_{-0.07}^{+0.00}(\text{th}) \text{ GeV}, \quad (6)$$

at NNLO<sub>approx</sub>, approximate NNLO, in perturbation theory. The quoted experimental uncertainty results from the propagation of the statistical and systematic errors in the data with account of error correlations whenever available. The theoretical uncertainty is estimated from the variation of the renormalization and factorization scales by a factor of 1/2 and 2 around the nominal value of  $\sqrt{m_c^2 + \kappa Q^2}$ , with  $\kappa = 4$  for the NC and  $\kappa = 1$  for the CC case. For consistency it has been checked that different scale choices do not deteriorate the statistical quality of the fit. Counting the charm mass  $m_c$  quoted in eqs. (5) and (6) and the value of the strong coupling constant determined to  $\alpha_s(M_Z) = 0.1134 \pm 0.0011$  at NNLO [25],

the global fit relies on the same 27 correlated parameters for PDFs as in the ABM11 analysis [25]. An additional theoretical uncertainty estimated to 0.07 GeV in eq. (6) arises from the incomplete knowledge of the massive NNLO coefficient functions derived in ref. [19] and parametrized as options A and B. The recent data on DIS open charm production [29] is shown in fig. 1 and the value of  $m_c(m_c)$  in eq. (6) provides the best description of the data. With  $\chi^2$  normalized by the number of data points ( $NDP$ ) the fit yields  $\chi^2/NDP = 61/52$  for the combined HERA charm data, cf. fig. 1.

Full control of the correlation with the PDFs is particularly important in order to check simultaneously the sensitivity to the strange-quark PDF in the CC case, because due to the Born process  $W^\pm s \rightarrow c$ , the charm mass parameter is correlated with strange-quark distribution. A recent analysis of CC fixed-target data in ref. [24] includes the NuTeV/CCFR data [30] together with the new high statistics NOMAD [31] and CHORUS data [32] into the fit. It has obtained [24]

$$m_c(m_c) = 1.222 \pm 0.024 (\text{exp.}) \text{ GeV}, \quad (7)$$

which is consistent with eq. (6) and the one of the ABM12 fit [26], but has a slightly improved experimental uncertainty due to the impact of the newly added NOMAD and CHORUS data.

One has to compare the numbers in eqs. (5), (6) and (7) with the world average of the PDG [9] quoted in the  $\overline{\text{MS}}$  scheme as  $m_c(m_c) = 1.275 \pm 0.025 \text{ GeV}$ , which includes lattice computations or analyses of experimental data with time-like kinematics from  $e^+e^-$ -collisions, e.g. with the help of QCD sum rules. It is therefore interesting to note that the DIS results in eqs. (5), (6) and (7) for hadronic processes with space-like kinematics are fully consistent with the PDG value, though with a slightly larger overall uncertainty.

In order to understand at least one source of the larger uncertainty, one should note that the QCD sum rules analyses typically assume the Bethke world average for the value of the strong coupling constant [33], which is  $\alpha_s(M_Z) = 0.1184 \pm 0.0007$  and therefore significantly larger than the ABM11 result [25], see also [34] and references therein. A recent determination from a charmonium QCD sum rules analysis [35] (see also [36] for an update) quotes a central value  $m_c(m_c) = 1.282 \pm 0.024 \text{ GeV}$  using the world average and parametrizes separately the dependence of  $m_c(m_c)$  on the value of  $\alpha_s(M_Z)$ . Using the ABM11 value  $\alpha_s(M_Z) = 0.1134$  instead one extracts from Table 15 in [35] a value of  $m_c(m_c) = 1.262 \pm 0.024 \text{ GeV}$ , i.e. a systematic shift downwards at the level on  $1\sigma$  statistical uncertainty. Similar findings have also been presented in [37]. This

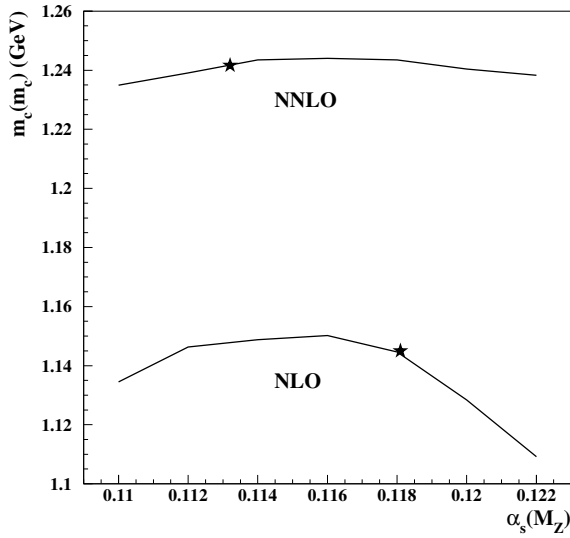


Figure 2: The values of  $m_c(m_c)$  obtained in the NLO and NNLO variants of the ABM11 fit with the combined HERA charm data [29] included and the value of  $\alpha_s(M_Z)$  fixed. The position of the star displays the result with the value of  $\alpha_s(M_Z)$  fitted [25]. (Figure from ref. [28])

indicates a potential bias with respect to the value of the strong coupling constant in QCD sum rule analysis from  $e^+e^-$ -collisions. Note that the DIS determinations in eqs. (5), (6) and (7) account for the full correlation of the dependence on  $m_c$  and  $\alpha_s$  through a simultaneous fit of these parameters. The correlation of the fitted value of  $m_c$  with the strong coupling constant  $\alpha_s(M_Z)$  is shown in fig. 2 which demonstrates a remarkable stability of the charm-quark mass both at NLO and NNLO for a variation of the value of  $\alpha_s(M_Z)$  in a wide range.

### 3. Bottom-quark mass

At asymptotically large scales  $Q \gg m_c, m_b$  the genuine DIS heavy-quark contributions in a FFNS with  $n_f = 3$  grow as  $\alpha_s(Q^2) \ln(Q^2/m^2)$  and can be resummed by means of standard renormalization group methods. This procedure leads to so-called heavy-quark PDFs in theories with effectively  $n_f = 4$  and  $n_f = 5$  light flavors, which are the appropriate descriptions for processes at LHC energies. The PDFs for charm- and bottom-quarks in 4- and 5-flavor schemes are generated from the light flavor PDFs in a 3-flavor FFNS as convolutions with massive operator matrix elements (OMEs), see e.g. [38]. The uncertainty on heavy-quark PDFs is therefore directly related to the accuracy of the quark masses  $m_c$  or

$m_b$ , which appear parametrically in the OMEs. This uncertainty can be significantly reduced through the use of the  $\overline{\text{MS}}$  scheme, which, of course, has to be applied also to the massive OMEs.

In the global fits of PDFs the heavy-quark masses are free parameters, which can be supplemented by the PDG constraint, though. In this way refs. [25, 26] have generated charm PDFs with comparable uncertainties to the one of ref. [38] (which has used the pole mass definition for  $m_c$ ). Using the value  $m_b(m_b) = 4.19 \pm 0.13$  GeV the uncertainty of the resulting bottom-PDF is, however, greatly reduced as shown in fig. 3. This improvement has an impact on LHC phenomenology, e.g., by allowing for precise predictions for the production of single-top-quarks.

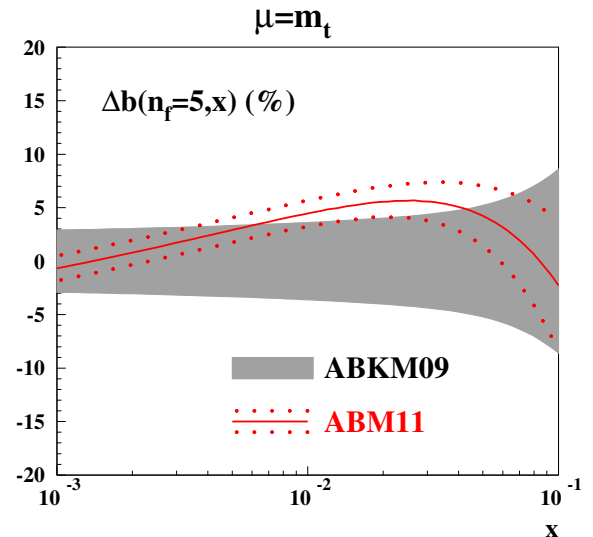


Figure 3: The  $b$ -quark PDF uncertainties obtained in the ABM11 fit [25]. The dotted (red) lines denote the  $\pm 1\sigma$  band of relative uncertainties (in percent) and the solid (red) line indicates the difference in the central prediction resulting from the change of the mass scheme and using  $m_b(m_b) = 4.19 \pm 0.13$  GeV. For comparison the shaded (grey) area represents the uncertainties in the ABKM fit [38] which has used pole masses. (Figure from ref. [25])

For long time the available DIS data on bottom-quark production has displayed little sensitivity on the mass parameter obstructing a direct determination of  $m_b(m_b)$ . Very recently, a new measurement of bottom production in DIS at HERA has been released [39]. Using the methods of ref. [23], this has allowed for a first measurement of the bottom-quark mass  $m_b(m_b)$  in a DIS scattering reaction. Ref. [39] reports

$$m_b(m_b) = 4.07 \pm 0.15(\text{exp})_{-0.05}^{+0.08}(\text{th}) \text{ GeV}, \quad (8)$$

at NLO, which is in very good agreement with the world average of the PDG [9] quoted in the  $\overline{\text{MS}}$  scheme as  $m_b(m_b) = 4.18 \pm 0.03$  GeV. Using the results of [25, 26] a determination of  $m_b(m_b)$  at NNLO is forthcoming.

#### 4. Top-quark mass

Since the discovery of the top-quark almost 20 years ago the mass of the heaviest elementary particle currently known has been measured with an ever increasing and, by now, with unprecedented precision. The top-quark mass is a fundamental parameter of the Standard Model (SM) and the precise value is indispensable for predictions of cross sections at the LHC. Moreover, in the absence of direct evidence for new physics beyond the SM, precision theory predictions confronted with precision measurements have become an important area of research for self-consistency tests of the SM or in searching for new physics phenomena. This has been the motivation for significant progress, both on the theoretical and the experimental side, in addressing issues arising in precision top-quark mass determinations, see, e.g., [34, 40] for reviews of recent activities.

Here, two examples are given, where the numerical value of the top-quark mass  $m_t$  directly affects relevant physics interpretations. In fig. 4 the current experimental results for the  $W$ -boson mass  $M_W$  and the top-quark mass  $m_t$  are shown in comparison with the theory predictions of the SM and its minimal supersymmetric extension (MSSM) for a range of Higgs boson masses  $M_H$ , see, e.g., [41]. The plot indicates consistency of the values for the various mass parameters  $M_W$ ,  $m_t$  and  $M_H$  at the level of  $1\sigma$  uncertainties within the SM. In fig. 5 the direct impact of the top-quark mass on the Higgs sector is illustrated. Regions of stability of the electroweak vacuum in the  $m_t$  and  $M_H$  plane are plotted, which can be obtained from extrapolating the SM up to the Planck scale, see, e.g., [42, 43, 44, 45, 46]. Thus, at high scales the existence of a well-defined minimum of the Higgs potential that can induce breaking of the electroweak symmetry, depends crucially on the precise numerical value of  $m_t$ .

A variety of methods for top-quark mass extractions has been proposed thus far, see, e.g., [34, 40], which use a number of distinct observables. Examples include determinations of  $m_t$  from the total cross section, or its extraction from the distribution of the invariant mass of a lepton and a  $b$ -jet, see, e.g., [48, 49] and [50, 51], respectively.

With enough statistics, as expected from the LHC runs at increased collision energy  $\sqrt{s} = 13$  TeV, also exclusive observables with reconstructed top-quarks come

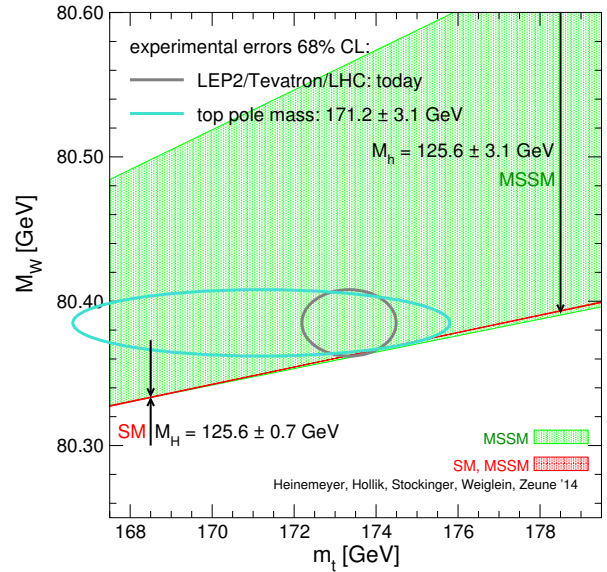


Figure 4: Current experimental results for  $M_W$  and  $m_t^{\text{pole}}$  and their  $1\sigma$  uncertainties in comparison with the SM (red band) and the MSSM prediction (light-shaded green band). (Figure courtesy S.Heinemeyer, cf. ref. [41]).

into focus. The (normalized) differential distribution of the  $t\bar{t} + 1$ -jet cross section with respect to the invariant mass of the  $t\bar{t} + 1$ -jet system displays very good sensitivity to  $m_t$ ,  $\mathcal{S} \sim 10 \dots 20$  in eq. (3) depending on the kinematical region and can, potentially, lead to very precise values for  $m_t$ , see [52].

All those methods employ mostly the pole mass scheme. The  $1S$  mass and the  $PS$  mass have been considered in applications to hadro-production of top-quark pairs in [53, 54]. In the sequel we will discuss the determination of the running mass in the  $\overline{\text{MS}}$  scheme and  $m_t$  from reconstructed kinematics as well as the relation of those mass parameters to the pole mass  $m_t^{\text{pole}}$ .

The running mass in the  $\overline{\text{MS}}$  scheme has so far been used in theory predictions for the inclusive cross section [21, 22] or for differential distributions in [56]. Such (semi-)inclusive observables are known with good precision, i.e., to NLO in perturbative QCD in the case of differential distributions [57, 58] or even to NNLO in the case of the inclusive cross section [59, 60, 61, 62], see also [63, 64, 65] for approximate NNLO differential cross sections. These computations are typically carried out in the pole mass scheme so that eq. (1) can be employed to relate  $m_t^{\text{pole}}$  to the  $\overline{\text{MS}}$  mass. For theory predictions in terms of the  $\overline{\text{MS}}$  mass the perturbative expansion in the strong coupling converges significantly faster. At the same time, the residual scale dependence as a measure of the remaining theoretical uncertainty is

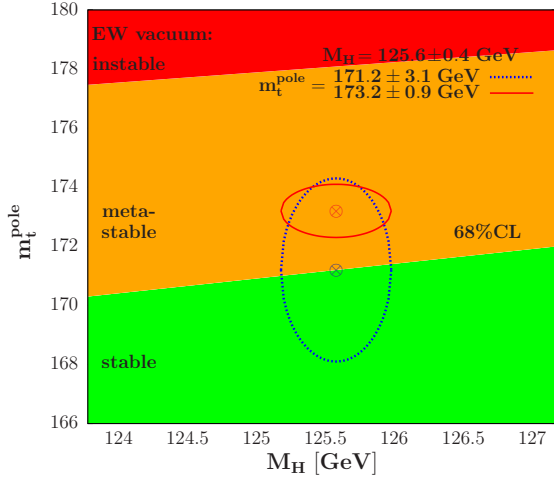


Figure 5: Ellipses for the  $1\sigma$  uncertainties in the  $[M_H, m_t^{\text{pole}}]$  plane with Higgs mass  $M_H = 125.6 \pm 0.4$  GeV and  $\alpha_s(M_Z) = 0.1187$  confronted with the areas in which the SM vacuum is absolutely stable, meta-stable and unstable up to the Planck scale. (Figure from ref. [47]).

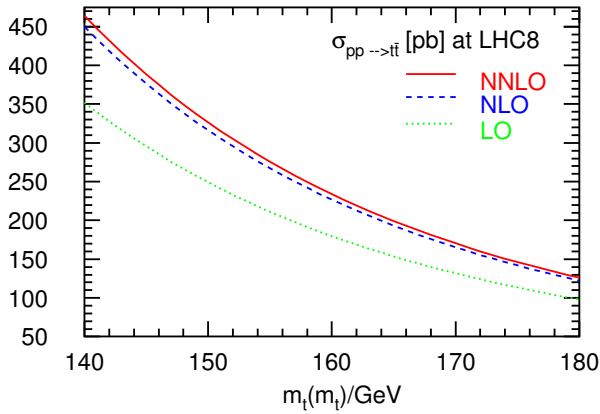


Figure 6: The LO, NLO and NNLO QCD predictions for the  $t\bar{t}$  total cross section at the LHC ( $\sqrt{s} = 8$  TeV) as a function of the top-quark mass in the  $\overline{\text{MS}}$  scheme  $m_t(m_t)$  at the scale  $\mu = m_t(m_t)$  with the ABM12 PDFs. (Figure from ref. [26]).

much improved when using the  $\overline{\text{MS}}$  mass in contrast to the pole mass  $m_t^{\text{pole}}$ .

These findings are illustrated in figs. 6 – 9. The theory predictions for inclusive top-quark pair production with the  $\overline{\text{MS}}$  and the pole mass are compared in figs. 6 and 7. The result in terms of the  $\overline{\text{MS}}$  mass  $m_t(m_t)$  displays a much improved convergence as the higher order corrections are successively added. The corresponding scale dependence is shown in figs. 8 and 9 and the predictions with the  $\overline{\text{MS}}$  mass exhibit a much better scale stability of the perturbative expansion. It is also inter-

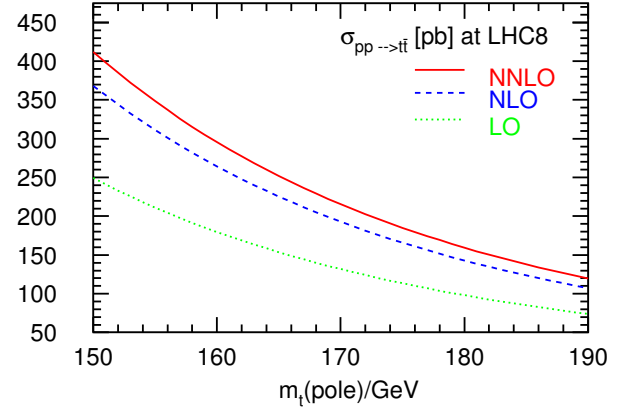


Figure 7: Same as fig. 6 for the top-quark mass in the on-shell scheme  $m_t^{\text{pole}}$  at the scale  $\mu = m_t^{\text{pole}}$ . (Figure from ref. [26]).

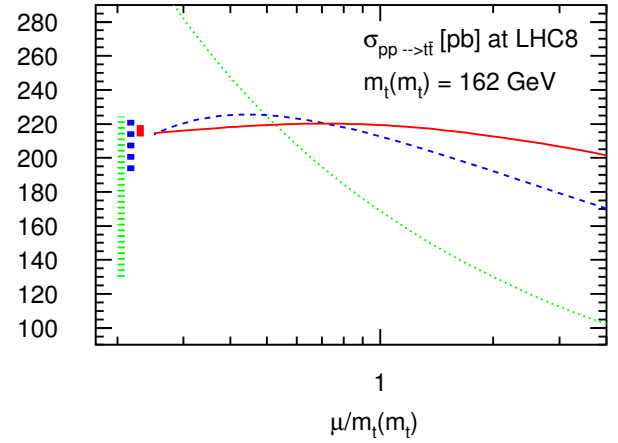


Figure 8: The scale dependence of the LO, NLO and NNLO QCD predictions for the  $t\bar{t}$  total cross section at the LHC ( $\sqrt{s} = 8$  TeV) for a top-quark mass  $m_t(m_t) = 162$  GeV in the  $\overline{\text{MS}}$  scheme with the ABM12 PDFs and the choice  $\mu = \mu_r = \mu_f$ . The vertical bars indicate the size of the scale variation in the standard range  $\mu/m_t(m_t) \in [1/2, 2]$ . (Figure from ref. [26]).

esting to observe, that the point of minimal sensitivity where  $\sigma_{\text{LO}} \simeq \sigma_{\text{NLO}} \simeq \sigma_{\text{NNLO}}$  is located at scales  $\mu = \mathcal{O}(m_t(m_t))$ , i.e., it coincides with the natural hard scale of the process for the  $\overline{\text{MS}}$  mass in fig. 8, whereas it resides at fairly low scales,  $\mu \simeq m_t^{\text{pole}}/4 \simeq 45$  GeV for the pole mass predictions in fig. 9.

For the distribution in the invariant mass  $m^{\bar{t}t}$  of the top quark pair the same findings can be seen in figs. 10 and 11. For the  $\overline{\text{MS}}$  mass predictions the convergence is improved. Also the overall shape of the distribution changes in comparison to case of the pole mass, the peak becomes more pronounced, while the position of the peak remains stable against radiative corrections. This is essential for precision determinations of

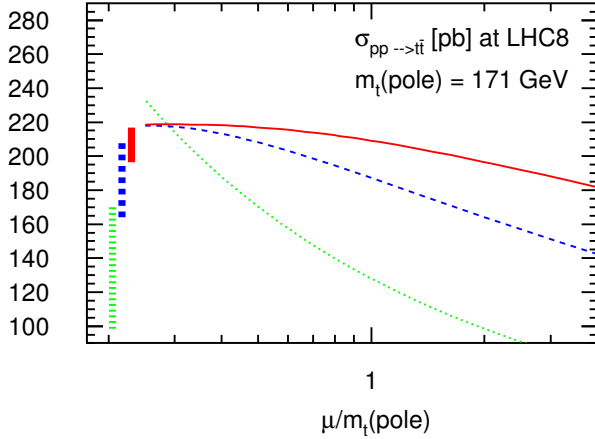


Figure 9: Same as fig. 8 for the top-quark mass in the on-shell scheme  $m_t^{\text{pole}} = 171$  GeV. The vertical bars indicate the size of the scale variation in the standard range  $\mu/m_t^{\text{pole}} \in [1/2, 2]$ . (Figure from ref. [26]).

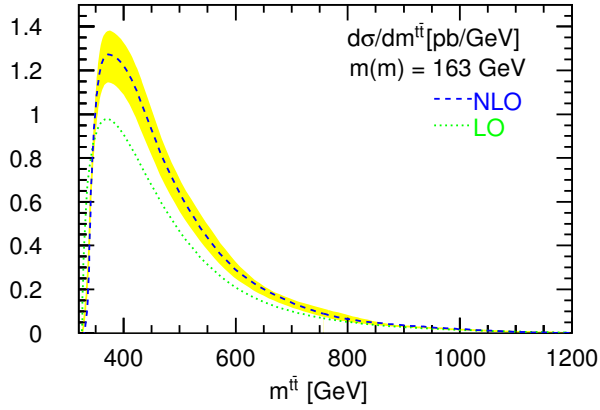


Figure 10: The differential cross section versus the invariant mass  $m^{\text{tt}}$  of the top-quark pair in the  $\overline{\text{MS}}$  mass scheme at the LHC with  $\sqrt{S} = 8$  TeV. The dotted (green) curves are the LO contributions, the dashed (blue) curves include NLO corrections and are obtained with the PDF set CT10 [55]. The scale dependence in the range  $\mu/m(m) \in [1/2, 2]$  is shown as a band around the NLO curve. (Figure from ref. [56]).

the  $\overline{\text{MS}}$  mass in specific kinematic regions of the invariant mass distribution from LHC data in the upcoming high-energy runs.

The results for the running mass imply, that experimental determinations of the mass parameter from the measured cross section can be performed with very good accuracy and a small residual theoretical uncertainty. This has been done in [26], where a fully correlated fit of the running mass from data for the total cross section at Tevatron and the LHC has given the value for the  $\overline{\text{MS}}$  mass at NNLO to

$$m_t(m_t) = 162.3 \pm 2.3 \text{ GeV}, \quad (9)$$

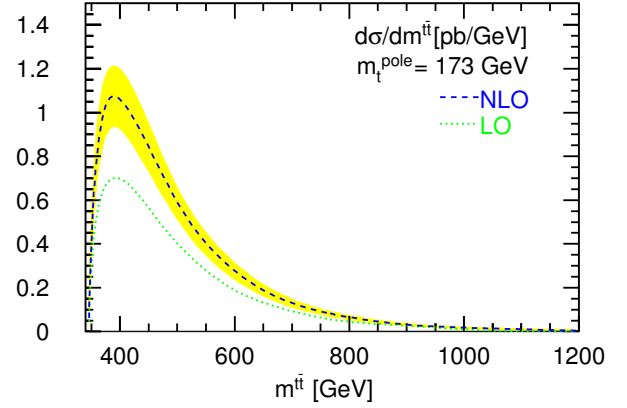


Figure 11: Same as fig. 10 for the top-quark mass in the pole mass scheme. The scale dependence in the range  $\mu/m_t^{\text{pole}} \in [1/2, 2]$  is shown as a band around the NLO curve. (Figure from ref. [56]).

with an error in  $m_t(m_t)$  due to the experimental data, the PDFs and the value of  $\alpha_s(M_Z)$ . An additional theoretical uncertainty from the variation of the factorization and renormalization scales in the usual range ( $\mu/m_t(m_t) \in [1/2, 2]$ ) is small,  $\Delta m_t(m_t) = \pm 0.7$  GeV. Eq. (9) is equivalent to the pole mass value of

$$m_t^{\text{pole}} = 171.2 \pm 2.4 \pm 0.7 \text{ GeV}, \quad (10)$$

using the known perturbative conversion eq. (1) at two loops. This is the value displayed in both plots of figs. 4 and 5, which show good consistency of the procedure and within the current uncertainties also with the top-quark mass values obtained from other determinations. The accuracy of a mass determination in this way is limited to order 1%, though, by the overall sensitivity of the total cross section to the mass parameter,  $S \sim 5$  in eq. (3).

## 5. Monte Carlo top-quark mass

The currently most precise measurement of the top-quark mass has been reported in [66] as the world combination of the experiments ATLAS, CDF, CMS and D0,

$$m_t = 173.34 \pm 0.76 \text{ GeV}. \quad (11)$$

This combination is based on determinations of  $m_t$  as a best fit to the mass parameter implemented in the respective Monte Carlo program used to generate the theory input. It is referred to as Monte Carlo (MC) top-quark mass definition and is, therefore, lacking a direct relation to a mass parameter in a well-defined renormalization scheme.

$m_t^{\text{MSR}}(1)$	$m_t^{\text{MSR}}(3)$	$m_t^{\text{MSR}}(9)$	$m_t(m_t)$	$m_{1\text{p}}^{\text{pole}}$	$m_{2\text{p}}^{\text{pole}}$	$m_{3\text{p}}^{\text{pole}}$
173.72	173.40	172.78	163.76	171.33	172.95	173.45

Table 1: Columns 1-3: Top-quark MSR masses at different scales. Column 4:  $\overline{\text{MS}}$  mass  $m_t(m_t)$  converted at  $O(\alpha_s^3)$  for  $\alpha_s(M_Z) = 0.1185$  from the MSR mass  $m_t^{\text{MSR}}(3 \text{ GeV})$ . Columns 5-7: Pole masses at 1, 2 and 3 loop converted from the  $\overline{\text{MS}}$  mass  $m_t(m_t)$ . All numbers are given in GeV units.

Nonetheless, the MC mass definition can be translated to a theoretically well-defined short-distance mass definition at a low scale with an uncertainty currently estimated to be of the order of 1 GeV, see [34, 67]. This translation uses the fact that multi-observable analyses like in [66] effectively assign a high statistical weight to the invariant mass distribution of the reconstructed boosted top-quarks, because of the large sensitivity of the system on the mass parameter, especially around the peak region.

The top-quark invariant mass distribution can be computed to higher orders in perturbative QCD, cf., figs. 10 and 11, and its peak position can also be described in an effective theory approach based on a factorization [68, 69] into a hard, a soft non-perturbative and a universal jet function. Each of those functions depends in a fully coherent and transparent way on the mass at a particular scale. The reconstructed top object largely corresponds to the jet function which is governed by a short-distance mass  $m_t^{\text{MRS}}$  at the scale of the top quark width  $\Gamma_t$ , see, e.g., [34, 67]. This line of arguments allows one to systematically implement proper short-distance mass schemes for the description of the MC mass in eq. (11), which can then indeed be converted to the pole mass.

Thus, the top-quark mass parameter  $m_t^{\text{MC}}$  is identified with a scale-dependent short-distance mass  $m_t^{\text{MSR}}(R)$  at low scales, cf. [67],

$$m_t^{\text{MC}} = m_t^{\text{MRS}}(3_{-2}^{+6} \text{ GeV}), \quad (12)$$

with an uncertainty  $\Delta m_t$  originating from the range of possible scales,  $R \simeq 1 \dots 9 \text{ GeV}$ . The value of  $\Delta m_t$  can be read off from Tab. 1 as  $\Delta m_t = {}_{-0.62}^{+0.32} \text{ GeV}$ . It should be emphasized, though, that this uncertainty is only an estimate of the conceptual uncertainty that is currently inherent in eq. (12). Very likely, the true corrections are not exactly calculable since a complete analytic control of the MC machinery is not feasible and the exact definition of the MC mass also depends on details of the parton shower, the shower cut and the hadronization model, see, e.g., [70].

Subsequently, there are two choices to convert  $m_t^{\text{MSR}}$  in eq. (12) to the pole mass  $m_t^{\text{pole}}$ . The first possibility applies the renormalization group to run  $m_t^{\text{MSR}}$  from the low scales,  $R \simeq 1 \dots 9 \text{ GeV}$ , up to  $R = m_t$  in order to

obtain the corresponding value for the  $\overline{\text{MS}}$  mass  $m_t(m_t)$ . This procedure effectively resums large logarithms. Afterwards,  $m_t(m_t)$  is then converted to the pole mass at a given order in perturbation theory. Tab. 1 illustrates this procedure for  $m_t^{\text{MSR}}(3 \text{ GeV}) = 173.40 \text{ GeV}$ , see [34] for an extensive documentation.

The second choice converts the short distance mass  $m_t^{\text{MSR}}$  at the low scales directly to the pole mass as shown in Tab. 2. This leads to relatively small corrections, however, the convergence of the perturbative expansion is poor and it is therefore disfavored. In the application of the one-, two- or three-loop conversion formula, the value of the mass parameter shifts by roughly  $\Delta m_t \sim 0.15 \text{ GeV}$  with every additional order. This is due to large logarithms which need to be resummed via the renormalization group equation [71].

$m_t^{\text{MSR}}(3)$	$m_{1\text{p}}^{\text{pole}}$	$m_{2\text{p}}^{\text{pole}}$	$m_{3\text{p}}^{\text{pole}}$
173.40	173.72	173.87	173.98

Table 2: Column 1: Top-quark MSR mass at  $R = 3 \text{ GeV}$ . Columns 2-4 show the 1, 2 and 3 loop pole masses converted from the MSR mass  $m_t^{\text{MRS}}(3 \text{ GeV})$ . All numbers are given in GeV units.

In summary, this leads to the following result for the pole mass, which corresponds to the MC mass in eq. (11),

$$m_t^{\text{pole}} = 173.39 \pm 0.76 \text{ GeV (exp)} + \Delta m_{\text{th}}, \quad (13)$$

where the small increase by 0.05 GeV in the central value compared to eq. (11), is due to the shift of the three-loop pole mass with respect to  $m_t^{\text{MSR}}(3 \text{ GeV})$  in Tab. 1. The theoretical uncertainty can be estimated to

$$\Delta m_{\text{th}} = {}_{-0.62}^{+0.32} \text{ GeV} (m_t^{\text{MC}} \rightarrow m_t^{\text{MSR}}(3 \text{ GeV})) + 0.50 \text{ GeV} (m_t(m_t) \rightarrow m_t^{\text{pole}}), \quad (14)$$

where, as indicated, the first part of the uncertainty is due to the scale choices when relating the MC mass to the short-distance mass and is subject to the qualifications mentioned above. The second part of the uncertainty,  $\Delta m_t = +0.50 \text{ GeV}$ , estimates the unknown higher order corrections in the conversion of the  $\overline{\text{MS}}$  to the pole mass. Those corrections are positive and the quoted value for  $\Delta m_t$  is taken as the difference between the two-loop and the three-loop conversion, see column 6 and 7

in Tab. 1. This part can definitely be diminished once the relation of the pole to the  $\overline{\text{MS}}$  mass, i.e., the respective coefficients  $a_{nk}$  in eq. (1), are known to four loops in QCD.

Altogether, the additional uncertainties in eq. (14) are sizeable and have not been addressed in [66] when interpreting the experimental measurement of the top-quark mass in eq. (11). The theory uncertainties are not uncorrelated, i.e., the linear sum  $\Delta m_{\text{th}} = {}^{+0.82}_{-0.62}$  GeV in eq. (14) should be combined in quadrature with the experimental error in eq. (13) leading to  $m_t^{\text{pole}} = 173.39^{+1.12}_{-0.98}$  GeV for the MC mass in eq. (11).

## 6. Summary

In QCD an unambiguous definition of the mass parameter requires the choice of a renormalization scheme, which is conventionally taken to be the pole mass, although this has its short-comings due to the renormalon ambiguity. A theoretically well-defined determination of the quark mass as a short-distance mass is possible in QCD even to NNLO by using inclusive observables like structure functions in DIS for charm- or bottom-quarks or the total cross section for hadro-production of top-quark pairs. This has the advantage that the theory predictions in terms of the  $\overline{\text{MS}}$  mass converge faster at higher orders and are less affected by scale variations. Results for the determination of the quark masses in this way have been presented for charm in eqs. (5), (6) and (7), for bottom in eq. (8) and for top in eqs. (9) and (10).

The use of running masses in global analyses of PDFs together with theory predictions for the DIS heavy-quark scattering processes in the FFNS allows for a precise description of the data and well-defined extractions of the mass parameters for charm- and bottom-quarks which are compatible with the world average. The charm-quark masses reported in eqs. (5), (6) and (7) have been obtained by keeping the full correlation of the dependence on all fit parameters.

The top-quark mass is an outstanding parameter in the SM. Its numerical value is important for many precision tests of the model at current collider energies as well as for possible extrapolations to high energies. The top-quark mass parameter measured via kinematical reconstruction from the top-quark decay products by comparison to MC simulations, termed the MC mass, is not identical to the pole mass. However, the measured values can be converted to the pole mass provided certain assumption on the relation of the MC mass to a short-distance mass at a low scale are made. This conversion leads to an additional uncertainty of the order of 1

GeV as quantified in eqs. (12)–(14). Within the current accuracies, all those determinations show good consistency. Further efforts both in theory and experiment are required though, to reduce the uncertainty.

## Acknowledgments

Collaborations with S. Alekhin, J. Blümlein, M. Dowling, U. Langenfeld, K. Lipka, N. Lo Presti, H. Kawamura, P. Uwer and A. Vogt are gratefully acknowledged.

## References

- [1] I. I. Bigi, M. A. Shifman, N. Uraltsev, and A. Vainshtein, *Phys.Rev.* **D50**, 2234 (1994), arXiv:hep-ph/9402360.
- [2] M. Beneke and V. M. Braun, *Nucl.Phys.* **B426**, 301 (1994), arXiv:hep-ph/9402364.
- [3] M. C. Smith and S. S. Willenbrock, *Phys.Rev.Lett.* **79**, 3825 (1997), arXiv:hep-ph/9612329.
- [4] A. H. Hoang, Z. Ligeti, and A. V. Manohar, *Phys.Rev.* **D59**, 074017 (1999), arXiv:hep-ph/9811239.
- [5] A. Hoang and T. Teubner, *Phys.Rev.* **D60**, 114027 (1999), arXiv:hep-ph/9904468.
- [6] M. Beneke, *Phys.Lett.* **B434**, 115 (1998), arXiv:hep-ph/9804241.
- [7] K. Chetyrkin and M. Steinhauser, *Nucl.Phys.* **B573**, 617 (2000), arXiv:hep-ph/9911434.
- [8] K. Melnikov and T. v. Ritbergen, *Phys.Lett.* **B482**, 99 (2000), arXiv:hep-ph/9912391.
- [9] Particle Data Group, K. Olive *et al.*, *Chin.Phys.* **C38**, 090001 (2014).
- [10] S. Alekhin and S. Moch, (2011), arXiv:1107.0469.
- [11] S. Moch, *PoS LL2014*, 054 (2014), arXiv:1408.6080.
- [12] T. Gottschalk, *Phys.Rev.* **D23**, 56 (1981).
- [13] M. Gluck, S. Kretzer, and E. Reya, *Phys.Lett.* **B380**, 171 (1996), arXiv:hep-ph/9603304.
- [14] M. Buza and W. van Neerven, *Nucl.Phys.* **B500**, 301 (1997), arXiv:hep-ph/9702242.
- [15] S. Moch, (2013), unpublished.
- [16] J. Blümlein, A. Hasselhuhn, and T. Pföh, *Nucl.Phys.* **B881**, 1 (2014), arXiv:1401.4352.
- [17] E. Laenen, S. Riemersma, J. Smith, and W. van Neerven, *Nucl.Phys.* **B392**, 162 (1993).
- [18] N. Lo Presti, H. Kawamura, S. Moch, and A. Vogt, *PoS DIS2010*, 163 (2010), arXiv:1008.0951.
- [19] H. Kawamura, N. Lo Presti, S. Moch, and A. Vogt, *Nucl.Phys.* **B864**, 399 (2012), arXiv:1205.5727.
- [20] J. Ablinger *et al.*, (2014), arXiv:1409.1135.
- [21] U. Langenfeld, S. Moch, and P. Uwer, *Phys.Rev.* **D80**, 054009 (2009), arXiv:0906.5273.
- [22] M. Aliev *et al.*, *Comput.Phys.Commun.* **182**, 1034 (2011), arXiv:1007.1327.
- [23] S. Alekhin and S. Moch, *Phys.Lett.* **B699**, 345 (2011), arXiv:1011.5790.
- [24] S. Alekhin *et al.*, (2014), arXiv:1404.6469.
- [25] S. Alekhin, J. Blümlein, and S. Moch, *Phys.Rev.* **D86**, 054009 (2012), arXiv:1202.2281.
- [26] S. Alekhin, J. Blümlein, and S. Moch, *Phys.Rev.* **D89**, 054028 (2014), arXiv:1310.3059.
- [27] S. Alekhin, K. Daum, K. Lipka, and S. Moch, *Phys.Lett.* **B718**, 550 (2012), arXiv:1209.0436.

- [28] S. Alekhin, J. Blümlein, K. Daum, K. Lipka, and S. Moch, *Phys.Lett.* **B720**, 172 (2013), arXiv:1212.2355.
- [29] H1 Collaboration, ZEUS Collaboration, H. Abramowicz *et al.*, *Eur.Phys.J.* **C73**, 2311 (2013), arXiv:1211.1182.
- [30] NuTeV Collaboration, M. Goncharov *et al.*, *Phys.Rev.* **D64**, 112006 (2001), arXiv:hep-ex/0102049.
- [31] NOMAD, O. Samoylov *et al.*, *Nucl.Phys.* **B876**, 339 (2013), arXiv:1308.4750.
- [32] A. Kayis-Topaksu *et al.*, *New J.Phys.* **13**, 093002 (2011), arXiv:1107.0613.
- [33] S. Bethke *et al.*, (2011), arXiv:1110.0016.
- [34] S. Moch *et al.*, (2014), arXiv:1405.4781.
- [35] B. Dehnadi, A. H. Hoang, V. Mateu, and S. M. Zebarjad, *JHEP* **1309**, 103 (2013), arXiv:1102.2264.
- [36] B. Dehnadi, A. H. Hoang and V. Mateu, arXiv:1411.5597.
- [37] K. G. Chetyrkin *et al.*, *Phys.Rev.* **D80**, 074010 (2009), arXiv:0907.2110.
- [38] S. Alekhin, J. Blümlein, S. Klein, and S. Moch, *Phys.Rev.* **D81**, 014032 (2010), arXiv:0908.2766.
- [39] ZEUS Collaboration, H. Abramowicz *et al.*, *JHEP* **1409**, 127 (2014), arXiv:1405.6915.
- [40] A. Juste *et al.*, *Eur.Phys.J.* **C74**, 3119 (2014), arXiv:1310.0799.
- [41] S. Heinemeyer, W. Hollik, G. Weiglein, and L. Zeune, *JHEP* **1312**, 084 (2013), arXiv:1311.1663.
- [42] M. Holthausen, K. S. Lim, and M. Lindner, *JHEP* **1202**, 037 (2012), arXiv:1112.2415.
- [43] F. Bezrukov, M. Y. Kalmykov, B. A. Kniehl, and M. Shaposhnikov, *JHEP* **1210**, 140 (2012), arXiv:1205.2893.
- [44] G. Degrassi *et al.*, *JHEP* **1208**, 098 (2012), arXiv:1205.6497.
- [45] D. Buttazzo *et al.*, *JHEP* **1312**, 089 (2013), arXiv:1307.3536.
- [46] A. Andreassen, W. Frost, and M. D. Schwartz, (2014), arXiv:1408.0292.
- [47] S. Alekhin, A. Djouadi, and S. Moch, *Phys.Lett.* **B716**, 214 (2012), arXiv:1207.0980.
- [48] M. Beneke, P. Falgari, S. Klein, and C. Schwinn, *Nucl.Phys.* **B855**, 695 (2012), arXiv:1109.1536.
- [49] CMS Collaboration, S. Chatrchyan *et al.*, *Phys.Lett.* **B728**, 496 (2014), arXiv:1307.1907.
- [50] S. Biswas, K. Melnikov, and M. Schulze, *JHEP* **1008**, 048 (2010), arXiv:1006.0910.
- [51] G. Heinrich, A. Maier, R. Nisius, J. Schlenk, and J. Winter, *JHEP* **1406**, 158 (2014), arXiv:1312.6659.
- [52] S. Alioli *et al.*, *Eur.Phys.J.* **C73**, 2438 (2013), arXiv:1303.6415.
- [53] V. Ahrens, A. Ferroglia, M. Neubert, B. D. Pecjak, and L. L. Yang, *Phys.Lett.* **B703**, 135 (2011), arXiv:1105.5824.
- [54] P. Falgari, A. Papanastasiou, and A. Signer, *JHEP* **1305**, 156 (2013), arXiv:1303.5299.
- [55] J. Gao *et al.*, *Phys.Rev.* **D89**, 033009 (2014), arXiv:1302.6246.
- [56] M. Dowling and S. Moch, *Eur.Phys.J.* **C74**, 3167 (2014), arXiv:1305.6422.
- [57] J. M. Campbell and R. Ellis, *Nucl.Phys.Proc.Suppl.* **205-206**, 10 (2010), arXiv:1007.3492.
- [58] J. M. Campbell and R. K. Ellis, (2012), arXiv:1204.1513.
- [59] P. Bärnreuther, M. Czakon, and A. Mitov, *Phys.Rev.Lett.* **109**, 132001 (2012), arXiv:1204.5201.
- [60] M. Czakon and A. Mitov, *JHEP* **1212**, 054 (2012), arXiv:1207.0236.
- [61] M. Czakon and A. Mitov, *JHEP* **1301**, 080 (2013), arXiv:1210.6832.
- [62] M. Czakon, P. Fiedler, and A. Mitov, *Phys.Rev.Lett.* **110**, 252004 (2013), arXiv:1303.6254.
- [63] N. Kidonakis and B. D. Pecjak, *Eur.Phys.J.* **C72**, 2084 (2012), arXiv:1108.6063.
- [64] M. Guzzi, K. Lipka, and S. Moch, (2014), arXiv:1406.0386.
- [65] A. Broggio, A. S. Papanastasiou, and A. Signer, *JHEP* **1410**, 98 (2014), arXiv:1407.2532.
- [66] ATLAS Collaboration, CDF Collaboration, CMS Collaboration, D0 Collaboration, (2014), arXiv:1403.4427.
- [67] A. H. Hoang and I. W. Stewart, *Nucl.Phys.Proc.Suppl.* **185**, 220 (2008), arXiv:0808.0222.
- [68] S. Fleming, A. H. Hoang, S. Mantry, and I. W. Stewart, *Phys.Rev.* **D77**, 074010 (2008), arXiv:hep-ph/0703207.
- [69] S. Fleming, A. H. Hoang, S. Mantry, and I. W. Stewart, *Phys.Rev.* **D77**, 114003 (2008), arXiv:0711.2079.
- [70] P. Z. Skands and D. Wicke, *Eur.Phys.J.* **C52**, 133 (2007), arXiv:hep-ph/0703081.
- [71] A. H. Hoang, A. Jain, I. Scimemi, and I. W. Stewart, *Phys.Rev.Lett.* **101**, 151602 (2008), arXiv:0803.4214.